Iranian Journal of Science
https://doi.org/10.1007/s40995-024-01704-x

RESEARCH PAPER

Exploration of Photoactive Cd^{2+} Substitutions on V_2O_5 Nanoparticles and Their Catalytic Potential Against the Toxic Dye

A. Remila[1,2] · V. Shally[1,2] · C. Parvathiraja[3] · T. Darwin[4]

Received: 29 April 2024 / Accepted: 14 August 2024

Abstract

This study focuses on the synthesis and broad characterization of cadmium-doped vanadium pentoxide (Cd-doped V_2O_5) nanoparticles via the co-precipitation method, emphasizing the investigation of varying Cd^{2+} concentrations in V_2O_5. The synthesized nanoparticles were extensively characterized using X-ray diffraction (XRD), Fourier transform infrared spectroscopy (FTIR), and UV–Vis diffuse reflectance spectroscopy (UV–Vis DRS), revealing crystallite sizes ranging from 24 to 29 nm, identifying functional groups, and elucidating bandgap energies from 2.07 to 1.88 eV. Morphological analyses by field emission scanning electron microscopy (FE-SEM) and transmission electron microscopy (TEM) confirmed the presence of rod-like nanostructures without agglomeration. Energy-dispersive X-ray spectroscopy (EDX) confirmed successful Cd^{2+} integration into the V_2O_5 structure, while further characterization via X-ray photoelectron spectroscopy (XPS) and photoluminescence spectroscopy provided insights into valency, electron states, and material affinity. The catalytic activity of Cd-doped V_2O_5 nanoparticles in degrading Rhodamine B (Rh-B) dye was investigated under various conditions. pH variations notably influenced degradation rates, with acidic and alkaline environments demonstrating enhanced degradation capabilities due to electrostatic interactions and increased catalytic activity, respectively. Optimal catalytic efficiency was observed at a nanoparticle concentration of 10 mg, with declining efficiency attributed to surface area saturation at higher concentrations. Increasing dye concentrations inversely correlated with degradation percentages due to reduced hydroxyl radical formation. Reusability studies indicated consistent degradation efficiency over multiple cycles, suggesting promising applications of Cd-doped V_2O_5 nanoparticles in sustainable wastewater treatment.

Keywords Cadmium · Photoactivity · Vanadium pentoxide · OH radical · Photocatalysis · Visible light absorption

1 Introduction

In recent years, significant strides have been taken to develop doped nanoparticles, particularly in transition metal oxides, due to their capacity to enhance various properties such as optical, luminescent, magnetic, catalytic, and electrochemical characteristics. These advancements open up a plethora of potential applications spanning optoelectronic devices, photocatalysis, antimicrobial activities, supercapacitors, and gas sensors (Cleret de Langavant et al. 2024; Naeema et al. 2023; Salleh et al. 2024). The pressing concerns of environmental pollution and the energy crisis have led scientists to explore semiconductor photocatalysts as a solution for harvesting solar energy and mitigating environmental pollution (Salleh et al. 2024; Javdani-Mallak and Iman Salahshoori 2024). Rhodamine B, a common textile industry pollutant,

✉ V. Shally
shally.v@holycrossngl.edu.in

[1] PG & Research Department of Physics, Holy Cross College (Autonomous), Nagercoil 629004, India

[2] Affiliated to Manonmaniam Sundaranar University, Abishekapatti, Tirunelveli, Tamil Nadu 627012, India

[3] Department of Physics, Manonmaniam Sundaranar University, Abishekapatti, Tirunelveli, Tamil Nadu 627012, India

[4] Department of Mechanical Engineering, St. Xavier's Catholic College of Engineering, Chunkankadai, Nagercoil, Tamil Nadu 629003, India

Published online: 21 October 2024

underscores the urgency to sense and degrade hazardous chemicals below permissible limits to protect human health and the environment (Farooque Lanjwani et al. 2024; Bhakare et al. 2024; Boukoussa et al. 2024; Padervand et al. 2020; Ren et al. 2024; Dawi et al. 2023; Naderahmadian et al. 2023). The exploration of semiconductor materials, particularly transition metal oxides like V_2O_5, has garnered significant attention due to their promising photocatalytic properties. V_2O_5, with its unique structural characteristics and narrow band gap, presents exceptional performance across various applications (Vinothini et al. 2024a). The crystalline structure of V_2O_5, characterized by ordered two-dimensional layers, alongside its specific atomic arrangement and band alignment, make it highly promising for photocatalytic applications, particularly in harnessing solar energy (Bhuvaneswari et al. 2024; Zolfagharpour et al. 2024). However, early studies utilizing V_2O_5 derived from raw vanadium ore revealed limited photocatalytic performance. This spurred advancements in synthesis methodologies, leading to the exploration of various fabrication techniques including hydrothermal/solvothermal processes, sol–gel methods, electrodeposition, and high-temperature calcination (Zolfagharpour et al. 2024; Kočišová et al. 2024; Morsy et al. 2024). These approaches aim to tailor the properties of V_2O_5, optimizing its photocatalytic activity and overall performance. Despite its favourable attributes, such as high oxidation state, elevated decomposition temperature, and chemical stability, V_2O_5 faces challenges associated with its narrow band gap. This characteristic, while advantageous for efficient light absorption, also promotes the recombination of photoexcited electrons and holes, limiting the overall efficiency of the photocatalytic process (Wang et al. 2024; Jia et al. 2024). Addressing this issue has become a central focus of research efforts, driving the exploration of innovative strategies to enhance carrier separation and improve the overall efficacy of V_2O_5 -based photocatalysis. One promising approach involves doping V_2O_5 with transition metals, a strategy aimed at modifying its electronic structure to mitigate the recombination of charge carriers and thereby enhance its photocatalytic performance. Numerous transition metals including Ni, Fe, Cu, Mo, Zn and Cd have been investigated for their potential to enhance the photocatalytic activity of V_2O_5 (Sammed et al. 2024; Kishan Chand et al. 2024; Alqahtani et al. 2024; Sahoo et al. 2024; Ghannam et al. 2024; Vinothini et al. 2024b). However, challenges such as recombination of photoexcited electrons and holes hinder its photocatalytic efficiency. The introduction of dopants into metal oxides, including transition metals, induces surface defects which significantly influence their photoluminescent, catalytic, and antibacterial properties. Moreover, dopants can alter the optoelectronic properties, often shifting light absorption towards the visible spectrum. Doping V_2O_5 with transition metals offers a promising strategy to enhance its photocatalytic performance, with recent studies demonstrating significant improvements in photocatalytic degradation, especially in visible light-induced degradation of organic dyes. Heterogeneous photocatalytic advanced oxidation technologies (AOT) have emerged as effective methods for non-selective degradation of harmful chemicals into environmentally benign products. Textile industry wastewater, enriched with coloured dye effluents, primarily comprising azo compounds, poses significant environmental challenges (Alsharyani and Muruganandam 2024; Kumar et al. 2024; Gorsi et al. 2024; Chenchen et al. 2022). Semiconductor photocatalysts play a pivotal role in environmental protection by decomposing organic pollutants into water, CO_2, and mineral acids. For instance, recent studies have demonstrated that the co-doping of V_2O_5 with metals like Cd and Cu can lead to significant improvements in photocatalytic degradation, particularly in the visible light-induced degradation of organic dyes such as Congo red. Despite these advancements, challenges remain, including the wide band gap, low surface area, and high electron–hole pair recombination rate associated with V_2O_5 photocatalysts. Addressing these challenges will require continued innovation and interdisciplinary collaboration to unlock the full potential of V_2O_5 and other transition metal oxides for efficient solar-driven photocatalysis. Despite these advancements, challenges such as wide band gap, low surface Cadmium (Cd) doping of vanadium pentoxide (V_2O_5) nanoparticles serves as a versatile strategy in photocatalytic dye degradation (Qu et al. 2022; Xu et al. 2024).

Cadmium (Cd) doping of vanadium pentoxide (V_2O_5) nanoparticles serves as a versatile strategy in photocatalytic dye degradation. Firstly, it aims to enhance the photocatalytic activity of V_2O_5, thus improving its effectiveness in degrading organic dyes present in wastewater. Secondly, by tuning the optical, electronic, and structural properties of V_2O_5, Cd doping allows for tailored performance, crucial for optimizing photocatalytic efficiency. Thirdly, the incorporation of Cd has been found to increase the stability and durability of V_2O_5-based photocatalysts, ensuring sustained performance over multiple reaction cycles. Despite concerns about cadmium's toxicity, its controlled presence within doped materials mitigates risks, especially considering the benefits it offers in terms of improved photocatalytic activity. Additionally, Cd doping provides a means to control the synthesis process of V_2O_5 nanoparticles, influencing factors such as particle size, morphology, and surface area, which are crucial for enhancing photocatalytic performance.

2 Materials and Methods

2.1 Materials

Chemicals were procured from Sigma Aldrich, India, including Cadmium acetate ($C_4H_6CdO_4$), Ammonium metavanadate (NH_4VO_3), Ammonium solution and Ethylene glycol ($C_2H_6O_2$), all processed using double-distilled water during synthesis.

2.2 Synthesis of Cd-Doped V_2O_5 Nanoparticles

Cd-doped V_2O_5 nanoparticles were synthesized using the co-precipitation method. Ammonium metavanadate (NH_4VO_3) was dissolved in 100 mL of ethylene glycol at a concentration of 1 M. Various quantities (1 wt%, 5 wt%, and 10 wt%) of cadmium sources were added, and the mixture was vigorously stirred for two hours at 100 °C. To maintain a pH of 2–3, approximately 1 mL of ammonia solution was added dropwise. After cooling to room temperature, the resulting precipitates were centrifuged and washed with ethanol and distilled water, repeating the process five times. The sample was air-dried at room temperature and calcined at 600 °C for approximately two hours. The same process was followed for pure V_2O_5 nanoparticles without cadmium addition. The finely divided Cd-doped V_2O_5 nanoparticles obtained were utilized for further material examinations (Remila et al. 2024).

2.3 Materials Characterization

Material structural identification and crystalline phase were determined using an X-ray diffractometer ($2\theta = 10°–50°$, Cu-Kα radiation). Morphological changes were observed using HRTEM and FE-SEM with EDX. Functional groups and electronic transitions were analyzed using FT-IR spectrometer, UV-DRS, and Photoluminescence (PL) spectrofluorometer PC1 with an excitation wavelength of 330 nm. The bonding and binding between compounds were elucidated using XPS spectroscopy.

2.4 Photocatalytic Dye Degradation Activity

Dye degradation was examined using Cd-doped V_2O_5 catalyst under visible light (Xenon $>$ 400 nm) irradiation with Rh-B dye. Initially, 10 mg of nano-catalysts were impregnated in a 100 mL dye solution, followed by equilibration in dark conditions for 15 min with continuous magnetic stirring. The combined solutions were irradiated with visible light, and samples were taken out at regular intervals. After centrifugation to eliminate nanoparticles, dissociated dye molecules were observed using UV–Vis, and degradation percentage was calculated using the formula:

$$\text{Dye degradation } (\%) = (C0 - Ct)/C0 \times 100, \quad (1)$$

where C0 is initial dye solution absorbance and Ct is irradiated dye solution absorbance (Minisha et al. 2024).

To elucidate the active species involved in the photocatalytic degradation of dye, a scavenging analysis was conducted. This method aimed to identify and confirm the presence of super oxides, free radicals, and holes that participate in the photocatalytic process. Specific scavengers were employed to target each type of reactive species: triethanolamine (TEOA) for holes, p-benzoquinone (BQ) for superoxide radicals, and isopropyl alcohol (IPA) for hydroxyl radicals. Each scavenger was used at a concentration of 1 mmol/L during the reaction period. The decrease in degradation efficiency in the presence of each scavenger was used to infer the involvement of the corresponding reactive species. The results from the UV absorbance measurements allowed for the determination of the efficiency of the reactive species generated during the photocatalytic process.

3 Results and Discussion

3.1 XRD Analysis

The structural stability and crystallinity were determined from X-ray diffractometer and their findings were displayed from Fig. 1. The pure and different Cd concentrations of V_2O_5 nanoparticles are exposed the Fig. 1. The V_2O_5 nanoparticles exhibit peaks at 2-theta values of 15.82°, 22.27°, 26.54°, 29.81°, 31.47°, 32.45°, 34.64°, 39.93°, 41.26°, 42.34°, 43.14°, 43.74°, 45.82°, 46.26°, and 47.35°, corresponding to the planes (200), (010), (101), (310), (400), (011), (301), (311), (120), (220), (112), (510), (411), (501), and (660), confirming the orthorhombic structure of V_2O_5, consistent with the JCPDS card 86-2248. The Cd^{2+} substitutions over the V_2O_5 nanoparticles, occupied the V_2O_5 system and their concentrations are increased the intensities. The occupied intensities of Cd and their 2 theta peaks are 15.84°, 22.28°, 26.56°, 29.84°, 31.45°, 32.47°, 34.68°, 39.96°, 41.24°, 42.32°, 43.16°, 43.76°, 45.8°, 46.24°and 47.32° which are highly attribute the planes of (200), (010), (101), (310), (400), (011), (301), (311), (120), (220), (112), (510), (411), (501) and (660). The obtained peaks are confirmed the orthorhombic V_2O_5 system with the card of 86-2248 (JCPDS) (Bansal and Jain 2024; Nivetha et al. 2024). The peak modifications of shifting and intensity increments are emanates Cd^{2+} occupation and enhancement of the surface area (Nivetha et al. 2024). The disappeared and shifted peaks are

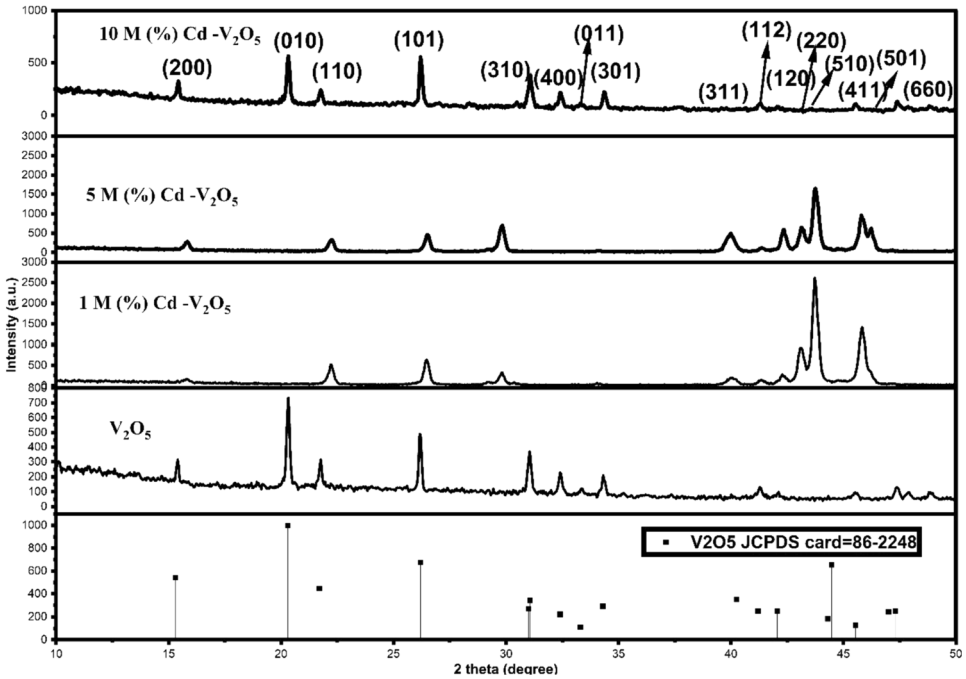

Fig. 1 X-ray diffraction patterns of JCPDS of V_2O_5, pure V_2O_5 and Cd (1, 5 and 10 M%) doped V_2O_5 nanoparticles

demonstrating the formation and substitution of the V_2O_5 lattice system and their Cd introduction on the V_2O_5 provides the peaks in V_2O_5 surfaces and there are no new peaks are appeared. The crystallite sizes of the synthesized nanoparticles were estimated using the Debye–Scherrer formula, resulting in sizes of 35 nm for pure V_2O_5 and 29 nm, 27 nm, and 24 nm for 1%, 5%, and 10% Cd-doped V_2O_5 nanoparticles, respectively. These size variations are attributed to differences in ionic radii and various phase substitutions within the synthesized materials.

3.2 FTIR Analysis

Figure 2 depicts the FTIR spectra of the synthesized pure and Cd-doped V_2O_5 nanoparticles, elucidating their role in stabilizing functional groups and forming V_2O_5 nanoparticles alongside Cd dopants at varying concentrations. The pure V_2O_5 nanoparticles exhibited the bands at 449 cm^{-1}, 519 cm^{-1}, 606 cm^{-1} and 823 cm^{-1} were identified as symmetric vibrations of V–O–V. The doping of Cd notably reduces the intensity of the OH peak across all concentrations. The presence of secondary OH vibrations and secondary C–O stretching of Cd-doped V_2O_5 nanoparticles is indicated by the narrow peak at 1010 and 1014 cm^{-1} (Abd El-Ghany et al. 2024). Primary and secondary stretching within a broad spectrum confirm the reduction and stabilization of the synthesized Cd-doped V_2O_5 nanoparticles, with prominent V–O stretching vibrations observed between 512–643 cm^{-1}, signifying metal and metal–oxygen interactions via chemisorbed molecules (Odhaib et al. 2024; Singh et al. 2024). The attachment of Cd metal to the inner sites of V_2O_5 nanoparticles is confirmed by peaks at 647–871 cm^{-1}, with the peaks shifting to lower/higher wavelengths at higher Cd concentrations, indicative of varying interactions between metals and metal oxide surfaces (Anand Pandarinath et al. 2024; Hussain et al. 2024). Higher Cd concentrations result in the disappearance of peaks, suggesting a strong interaction between Cd and V_2O_5 materials.

The dominance of Cd^{2+} in the V_2O_5 system reduces OH peak intensities in correlation with Cd doping, while secondary peaks from C–O and OH stretching of Cd-doped V_2O_5 nanoparticles are observed between 1000–1200 cm^{-1}. Cationic substitution, metal–oxygen interface, and oxygen stabilization are estimated from peaks at 770–980 cm^{-1}. Higher Cd^{2+} concentrations decrease peak intensities and shift them, penetrating the V_2O_5 system more effectively and confirming the absence of other elements at their interfaces (Hussain et al. 2024; Mishra 2024). The FTIR spectroscopy thus highlights the significant role of Cd^{2+} in influencing the functional groups, metal–oxygen interactions, and overall stabilization of synthesized Cd-doped V_2O_5 nanoparticles.

3.3 UV-DRS Analysis

The optical properties of the synthesized Cd-doped V_2O_5 nanoparticles were investigated through UV-DRS spectra, revealing crucial insights elucidated in Fig. 3a and b. The presence of Cd-doped V_2O_5 nanoparticles was confirmed by absorption edges ranging from 380 to 590 nm, indicating lower transitions in the visible region and suggestive

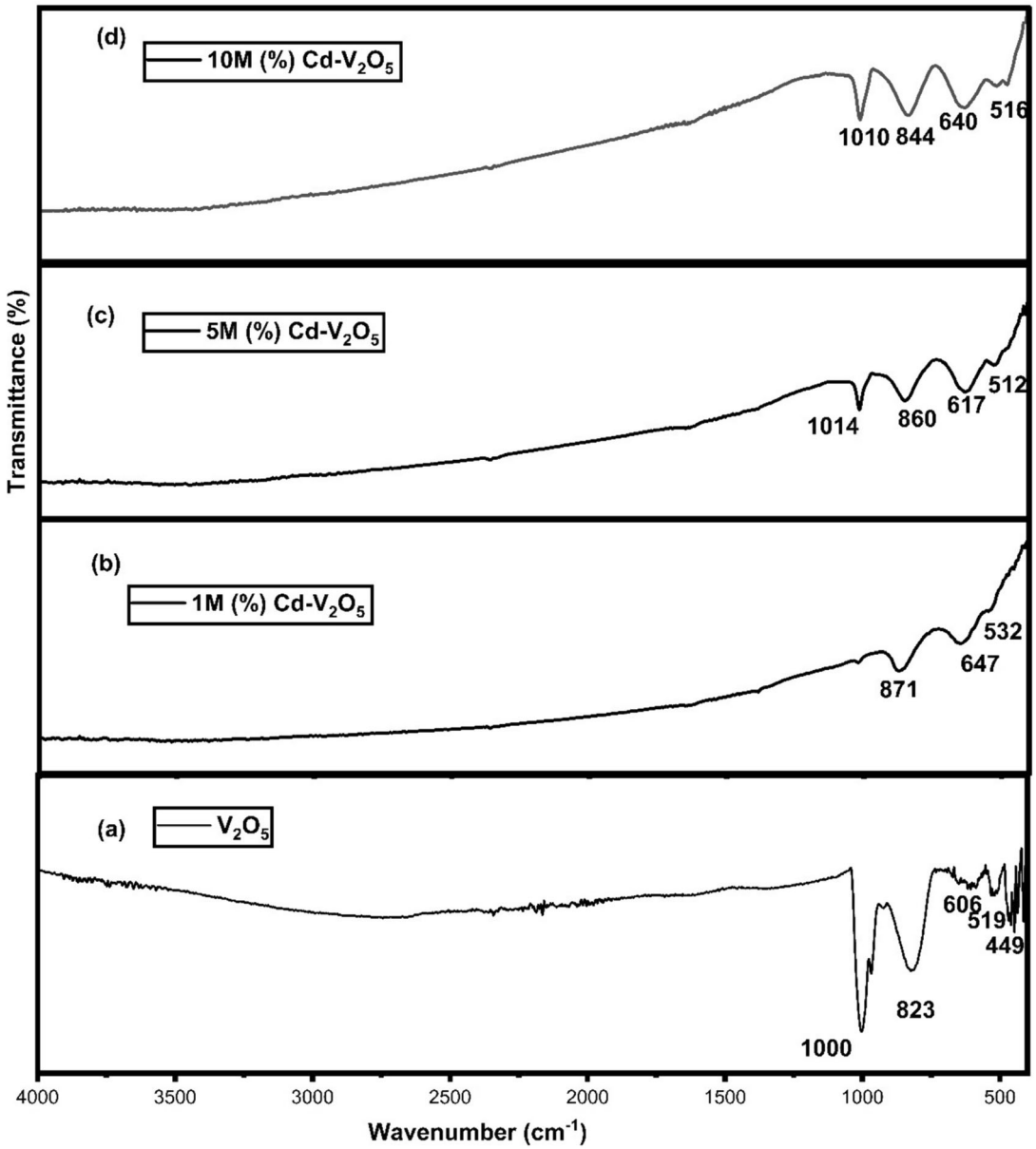

Fig. 2 FTIR spectra of pure (**a**) and Cd (**b**–**d**) (1, 5 and 10 M%) doped V_2O_5 nanoparticles

of charge transfer on the higher energy side. Cd cations effectively covered optical defects in the V_2O_5 nanoparticles, with valence band charges shifting to the conduction band upon Cd^{2+} introduction into the V_2O_5 lattice (Venkatesan et al. 2013; Raja et al. 2018). This transition resulted in decreased peak intensities and shifted wavelengths due to Cd metal integration.

Additionally, the presence of Cd induced optical activity in the V_2O_5 nanoparticles (Goudarzi and Soleymani 2019; Habibi and Rahmati 2014). Kubelka–Munk relations estimated bandgap values of 2.07 eV, 1.94 eV, and 1.88 eV for 1%, 5%, and 10% Cd-doped V_2O_5 nanoparticles, respectively, confirming decreased bandgaps conducive to charge carrier separation, visible light absorption, and e–h pair modification. Conspicuously, the 10 M(%) Cd-doped V_2O_5 samples exhibited lower intensity and wavelength transitions compared to other concentrations, with a bandgap difference of $\Delta Eg = 0.19$ eV. These energy gap values suggested enhanced light absorption, facilitating photo charge carrier generation and promoting photocatalytic activity. Moreover their findings emphasizing visible region absorptions indicative of oxygen vacancy and Cd^{2+} substitution, promoting electron accumulation and metal trapping (Habibi and Rahmati 2014; Rajalakshmi et al. 2014). Cationic substitution on the V_2O_5 nanoparticles led to peak shifts and decreased absorbance intensities,

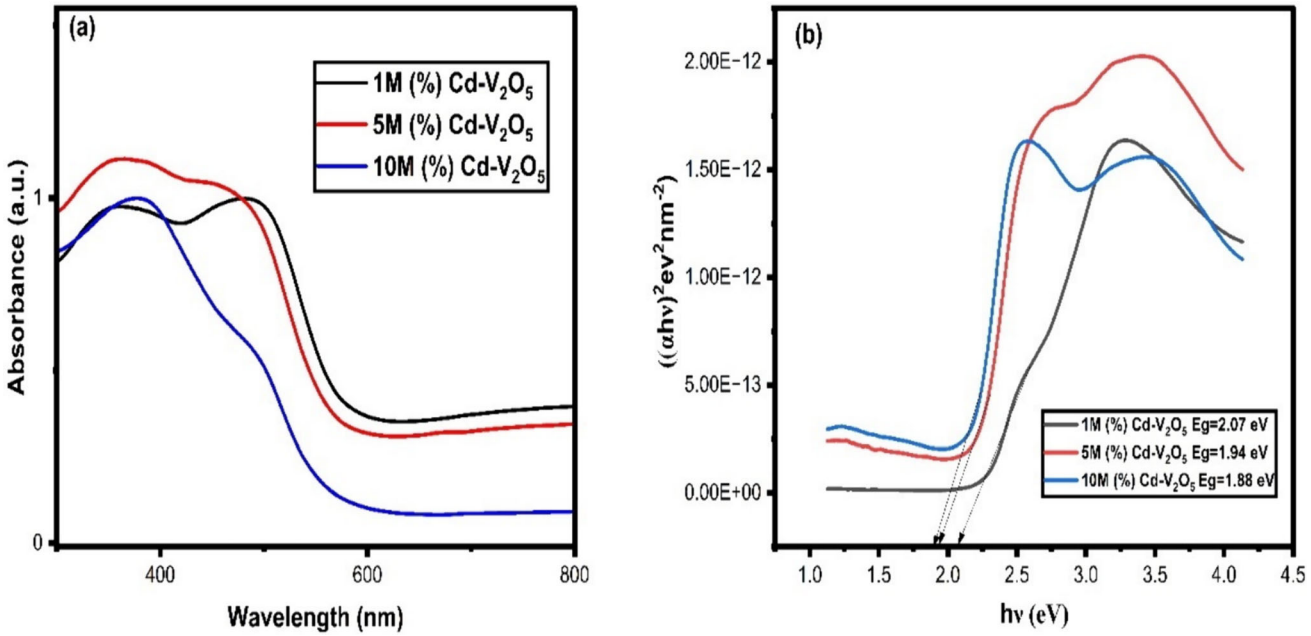

Fig. 3 **a** UV–Vis DRS spectra of the Cd (1, 5 and 10 M%) doped V_2O_5 nanoparticles and **b** bandgap spectrum

attributed to filled cationic vacancies and oxygen vacancy occupancy. This narrow bandgap and visible region absorption hold promising implications for wastewater treatment applications, accentuating the Cd-doped V_2O_5 nanoparticles' potential in catalytic and environmental remediation contexts.

3.4 Photoluminescence Analysis

In Fig. 4, Photoluminescence (PL) spectroscopy characterizes the luminescence properties of synthesized Cd-doped V_2O_5 nanoparticles, revealing distinct spectra at 510 nm and 660 nm. The primary peak at 510 nm originates from inter-band transitions, while the emission within the 620–690 nm range signifies transitions influenced by cadmium dopants, leading to increased oxygen vacancies and subsequent material stability alterations (Le et al. 2019; Wang et al. 2021; Chamarro et al. 1996; Vijayalakshmi and Venkataraj 2008). As cadmium concentrations escalate, there's a concurrent rise in PL intensity, attributed to structural rearrangements fostering elongated nanostructures. Notably, the peak within the 510–550 nm range experiences substantial enhancement, underscoring the profound impact of cadmium occupation on defects within V_2O_5 nanoparticles. The broad band at 680 nm indicates oxygen vacancies and their association with V^{4+} and Cd^{2+}. 10M% Cd-V_2O_5 is likely the optimal concentration for photocatalytic activity due to its balance between PL intensity and charge separation efficiency, as well as the potential for enhanced surface properties. This concentration provides a good compromise between maintaining enough charge carriers for photocatalysis and minimizing recombination losses. Cationic transitions over oxygen positions induce inter-band transitions, driving surface charge migrations, enhancing material stability, and promoting OH radical formations (Vijayalakshmi and Venkataraj 2008). Variation in Cd^{2+} concentrations alters oxygen arrangements relative to Cd^{2+} and V^{4+}. The initial peaks underscore charge carrier dynamics within metal–oxygen and metal-doped metal oxide nanoparticles. This luminescence augments our understanding of Cd-doped V_2O_5 nanoparticles' luminescence properties, paving the

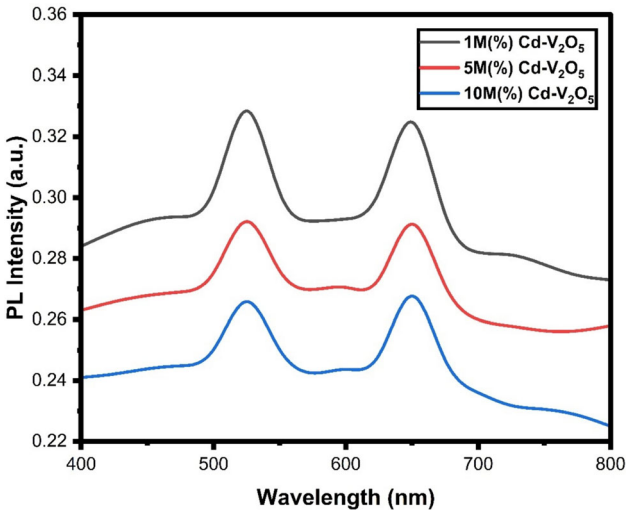

Fig. 4 Photoluminescence spectra of the Cd (1, 5 and 10 M%) doped V_2O_5 nanoparticles

way for enhanced applications in diverse fields with tailored functionalities.

3.5 FE-SEM with EDX Analysis

In Fig. 5a–f, the FE-SEM images and EDX spectrum displays the synthesized Cd-doped V_2O_5 nanoparticles structural characteristics and elemental composition. The incorporation of Cd into the V_2O_5 nanoparticles results in a distinct nanorod-like shape, with varying Cd concentrations leading to observable changes in morphology. At lower Cd concentrations, the nanoparticles exhibit conjoint rod structures with some agglomeration, while at 5 M%, elongated rod shapes with attached cubes are evident, indicating a transition from irregular shapes to more defined rods. High Cd concentrations yield reformed individual nanorod-like structures, indicative of Cd's influence on surface modification and area expansion, particularly evident when compared to lower Cd concentrations (Venu Gopal and Kamila 2017; Anandan and Rajendran 2011). Different Cd concentrations exhibit varied nanoparticle shapes, from semi-spherical to quasi-spherical, and rod and spherical shapes with sharp edges, indicating electron accumulation (Anandan and Rajendran 2011). EDX analysis confirms the presence of Cd, V, and O elements, with their respective peak values validating nanoparticle formation and revealing variations in peak percentages with different Cd concentrations. The addition of Cd alters the presence of V and O, with Cd anchoring onto the surface and infiltrating the nanoparticles, resulting in size enlargement, shape reformation, and modified peak distributions. Furthermore, Cd doping contributes to enhanced formation stability with reduced agglomeration. FE-SEM elucidates surface orientation, shape, and material distributions, while EDX aids in assessing material purity and identifying constituent elements. EDX spectroscopy corroborates the presence of Cd, V, and O, with their respective peaks reflecting their atomic properties and oxygen association. This integrated analysis provides valuable insights into the structural and compositional attributes of Cd-doped V_2O_5 nanoparticles, facilitating their potential applications in diverse fields.

3.6 HR-TEM Analysis

Figure 6 showcases TEM images of high concentrations of Cd^{2+} doped V_2O_5 nanoparticles, exhibiting spherical and rod-like shapes with regular surface distributions, and particle sizes ranging from 20 to 40 nm. These nano-meter scale images illustrate the assembly of Cd onto the V_2O_5 lattice, resulting in nanospheres and rod-like configurations, indicative of the interface between metal and metal oxide and subsequent surface modification processes (Jia et al. 2008; Jana et al. 2001). The dark coloration of the particles indicates oxygen displacement by cadmium and vanadium materials, with varying shades representing

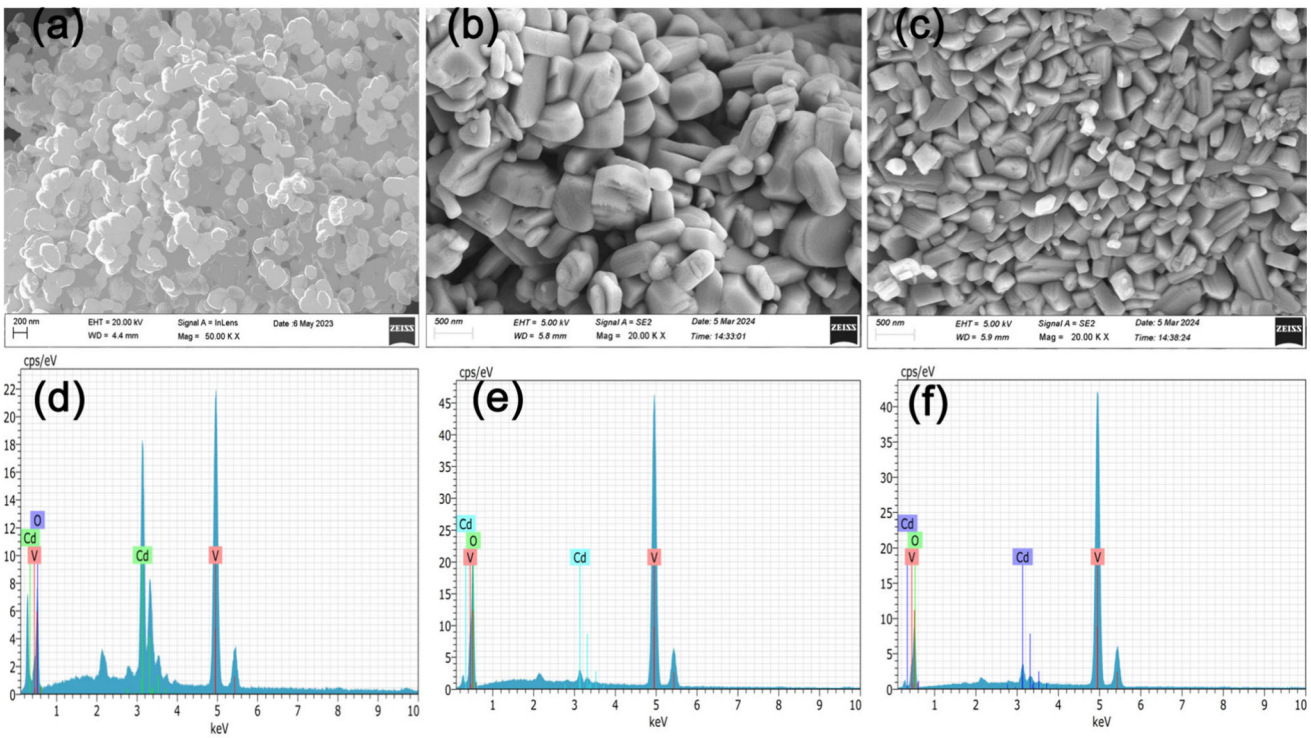

Fig. 5 FE-SEM images **a–c** of Cd (1, 5 and 10 M%) doped V_2O_5 nanoparticles and **d–f** EDX spectrum

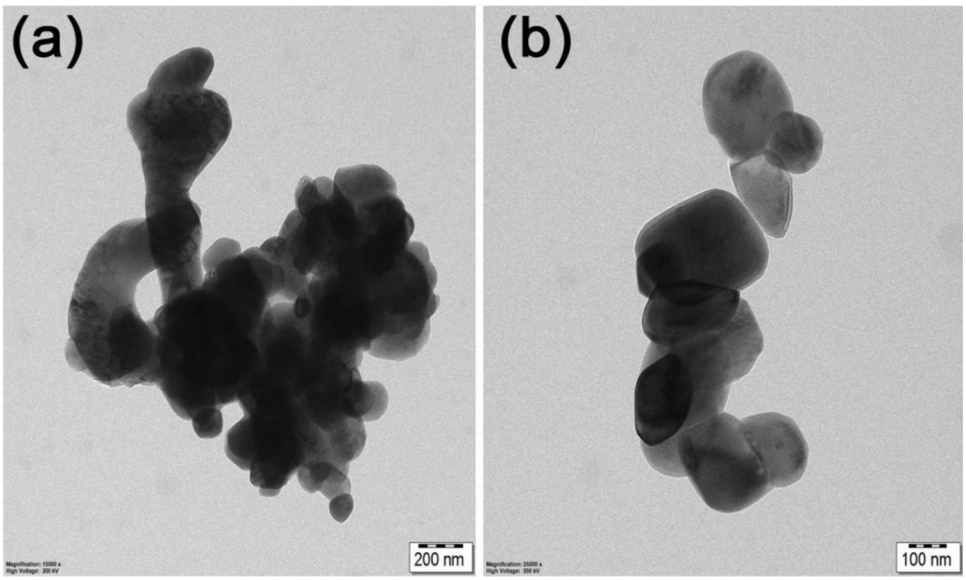

Fig. 6 HR-TEM images of Cd (10 M%) doped V_2O_5 nanoparticles

different atomic formations and oxygen vacancy regions. The polycrystalline nature of the synthesized nanoparticles facilitates a regular and repeating arrangement of atoms, resulting in even spacing between synthesized materials and contributing to the observed rod-like and spherical shapes of high Cd^{2+} concentration-doped V_2O_5 nanoparticles. The obtained particle size values of approximately 25 nm are consistent with X-ray crystallite size measurements, affirming the credibility of the observed structural modifications and their relationship with electron transfer dynamics between the metal and metal oxide phases (Jana et al. 2001). This electron transfer process enriches catalytic activity, highlighting the potential applications of Cd-doped V_2O_5 nanoparticles in various catalytic processes. This findings suggested that the structural evolution and potential applications of Cd-doped V_2O_5 nanoparticles in various fields, from catalysis to materials science.

3.7 XPS Analysis

X-ray photoelectron spectroscopy (XPS) was employed to analyse the material bond valency and binding energies of the synthesized Cd-doped V_2O_5 nanoparticles, as depicted in Fig. 7. The survey spectrum (Fig. 7a) confirms the formation of Cd^{2+} doped V_2O_5 nanoparticles, while the deep scanning of Cd-3d spectrum (Fig. 7b) reveals peak values at 404.28 eV and 410.98 eV, representing $Cd_{5/2}$ and $Cd_{3/2}$ valances associated with lattice oxygen and V material. V material binding energies at 516.58 eV and 523.88 eV denote $V2p_{3/2}$ and $V2p_{1/2}$ valences (Fig. 7c) (Le et al. 2012; Luo et al. 2010; Jenifer and Sriram 2023; Hota et al. 2007). The association of P orbitals with Cd and O bonds increases spacing/gap between materials due to their multivalent properties (Hota et al. 2007). Oxygen material valency at 529.38 eV indicates O-1s state, attributing peaks to Cd–O, V–O, and Cd–V–O interfaces (Fig. 7d). The material bonds between Cd, V, and O promote better lattice orientation, facilitating short-range visible light absorption, low-energy emission, and high reactive sites. Metal-doped metal oxide nanoparticles with multiple valency materials hold considerable promise in energy storage and catalytic-related applications. This integrated analysis enhances our understanding of Cd-doped V_2O_5 nanoparticles' structural and chemical properties, paving the way for their versatile applications in various fields.

3.8 Photocatalytic Activity

The photocatalytic dye degradation activity of Cd-doped V_2O_5 nanoparticles against Rh-B dye performed under visible light irradiation. The degradation details of various concentration Cd-doped V_2O_5 nanoparticles presented in Fig. 8. The raw dye absorbance is located at 554 nm, after that catalyst interaction with the help of light energy dye molecules breaking and their intensities are decreasing and peaks are shifted to higher wavelengths. The pure Rh-B dye degradation with the visible light is 8% in 60 min light irradiation. At 60 min time intervals high concentration of Cd-doped V_2O_5 nanoparticles demonstrated the 94% degradation of Rh-B dye and 1% and 5% of Cd-doped V_2O_5 nanoparticles displayed the 85% and 91% degradation respectively. The Cd penetration on the V_2O_5 lattice is varied and modified the transition energy between the bands. The Cd^{2+} is accumulated the electron migration, metal trapping and e–h pair lifetime. The low concentration of Cd degradation is 85%, promoting the electron shrinkage but their sacrificial surface and defect level was low compared to 1% and 5% of Cd-doped V_2O_5 nanoparticles.

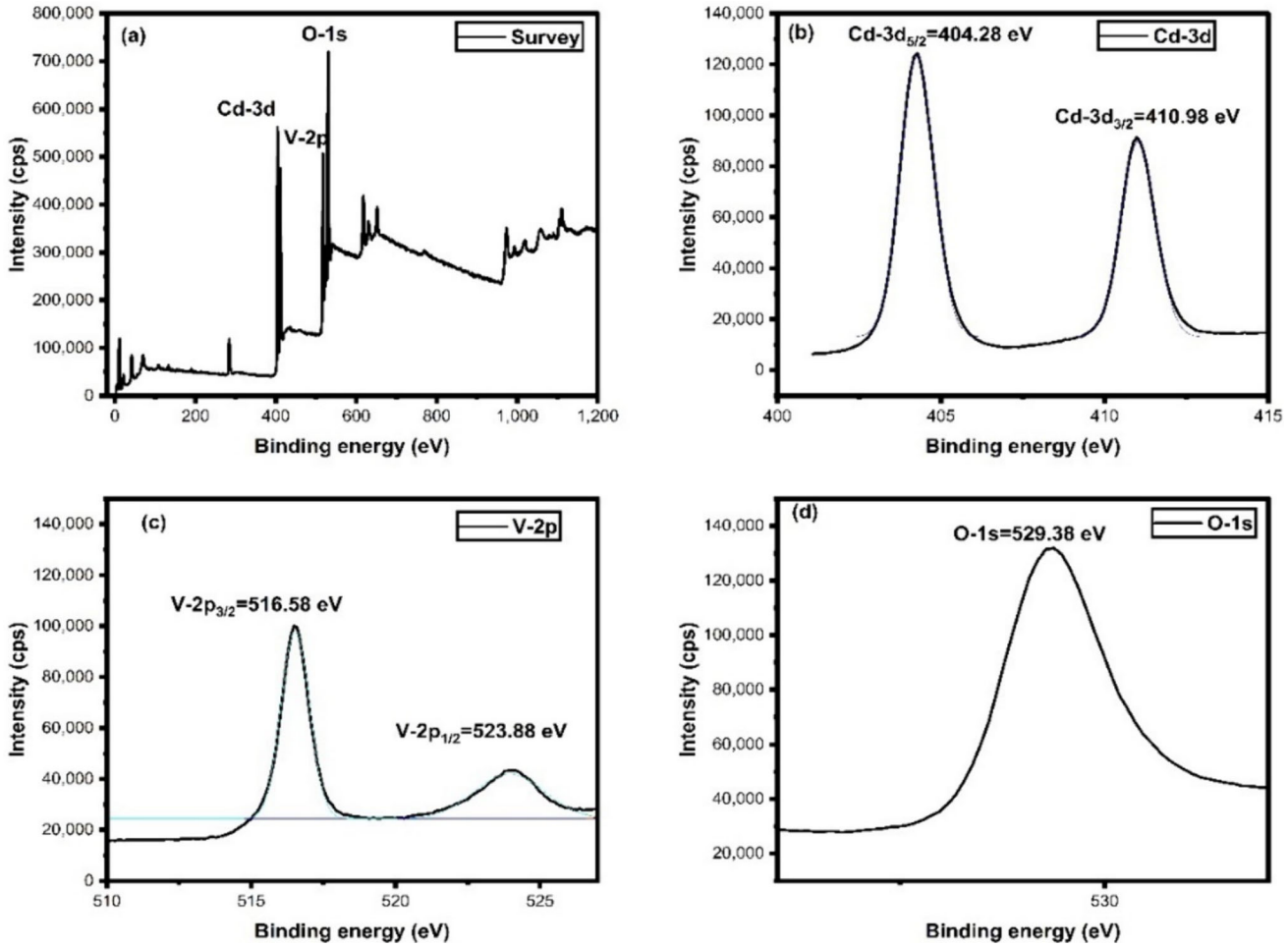

Fig. 7 XPS spectra of Cd-doped V_2O_5 (10 M%) nanoparticles: **a** survey spectrum, **b** Cd-3d spectrum, **c** V-2p spectrum and **d** O-1s spectrum

The Cd^{2+} substitution increased the surface area and induced the hot electrons which provokes the dissociated the dye molecules. The morphology, texture, shape and size of the materials are playing a vital role in the catalytic processes. V_2O_5 nanoparticles obtained the high work function material, wide bandgap and low visible light absorption. These property and shortcomings was overcome by substation of Cd-dopants. The dye degradation efficiency and kinetics of the Cd-doped V_2O_5 nanoparticles demonstrated in Fig. 8b and c. The photocatalytic dye degradation mechanism of Cd-doped V_2O_5 nanoparticles are displayed in Fig. 8 and their details are as follows:

$$Cd/V_2O_5 + h\nu \rightarrow Cd/V_2O_5(e^{-}CB + h^{+}VB) \quad (2)$$

$$e^{-}CB + O^2 \rightarrow {}^{\circ}O^{-2} \quad (3)$$

$$h^{+} + OH^{-} \rightarrow OH^{\circ} \quad (4)$$

$$OH^{\circ}/{}^{\circ}O^{-2} + \text{Dye} \rightarrow CO_2 + H_2O \quad (5)$$

The light irradiation over the Cd-doped V_2O_5 nanoparticles against Rh-B dye molecules promotes the band transition of electrons and holes and generated charge carriers. The interface between the Cd and V_2O_5 nanoparticles trapped the electrons and induced the oxygen defect. These productions are dissolved the oxygen molecules with OH radicals which generates the superoxide and hydroxide radicals. The discovery of these compounds neutralize the charge of the dye molecules and breakdown to the smaller non-toxic molecules (Shang et al. 2016).

The scavenging experiments revealed distinct reductions in photocatalytic efficiency with the addition of each scavenger, as shown in Fig. 9. The presence of TEOA, BQ, and IPA led to significant changes in the degradation rates, confirming the participation of holes, superoxide radicals, and hydroxyl radicals, respectively (Parvathiraja and Shailajha 2023). The Fig. 9 shows the degradation efficiency (%) of a catalyst in the presence of different quenching agents: BQ (benzoquinone), TEOA (triethanolamine), and IPA (isopropanol). The degradation efficiency of the catalyst, without any quenching agents, is 94%, indicating its optimal performance. In the presence of BQ, a superoxide radical scavenger, the degradation

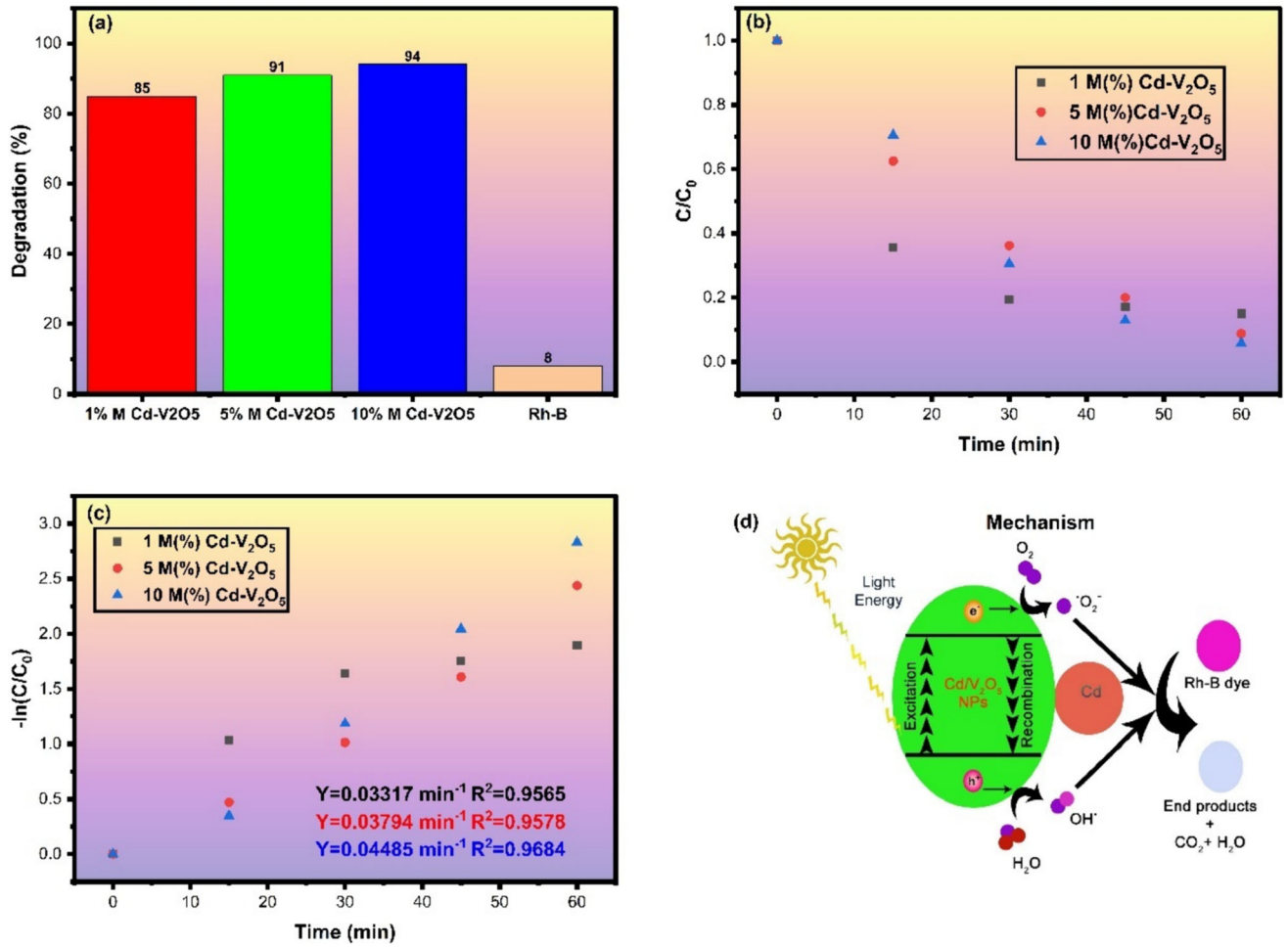

Fig. 8 Photocatalyst dye degradation of **a** percentage **b** C/C_0 and **c** pseudo- first-order kinetics and **d** mechanism of Cd-doped V_2O_5 nanoparticles against Rh-B dye

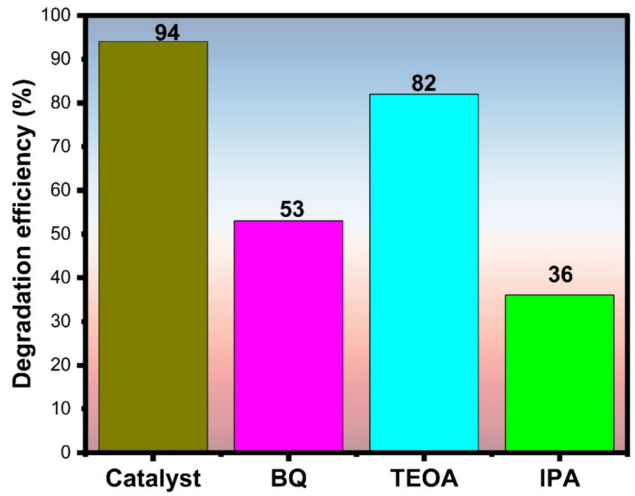

Fig. 9 Photocatalytic quenching analysis of Cd-doped V_2O_5 nanoparticles against Rh-B dye

efficiency drops significantly to 53%. This suggests that superoxide radicals play a crucial role in the catalytic degradation process, as BQ reduces the catalyst's effectiveness by scavenging these radicals. TEOA, acting as a hole scavenger, results in a less pronounced reduction in efficiency, down to 82%, indicating that while holes (positive charge carriers) are important, they are not as critical as superoxide radicals. IPA, a hydroxyl radical scavenger, causes a significant drop in degradation efficiency to 36%, highlighting the importance of hydroxyl radicals in the catalytic process. The presence of IPA reduces the availability of hydroxyl radicals, thus decreasing the efficiency.

The comparison of various metal oxide doping Cd material is compared with the present work as tabulated in Table 1. The table offers a complete investigation of various photocatalysts developed for the degradation of organic dyes under visible light irradiation, utilizing cadmium (Cd) as a support material. The diversity of photocatalysts, ranging from metal oxides like Bi_2WO_6, ZnO, and CeO_2 to semiconductor compounds such as $CuBi_2O_4$, TiO_2, and V_2O_5, highlights the broad spectrum of materials

explored to achieve efficient dye degradation (Song et al. 2015; Zhang and Zeng 2012; Gnanam and Rajendran 2018; Gnanam et al. 2021; Senobari and Nezamzadeh-Ejhieh 2018; Ghoderao et al. 2019; Suganya et al. 2019; Wang et al. 2015; Khan et al. 2024; Chandrasekar et al. 2023). Each entry in the table represents a distinct photocatalyst composition, paired with its corresponding performance in terms of degradation efficiency. The targeted organic dyes, including Rh-B, MB, CR, and MO, span a range of degradation efficiencies from 63 to 90.89%, indicating the varying effectiveness of the photocatalysts in dye degradation. This variation can be attributed to factors such as photocatalyst composition, surface area, and bandgap energy, all of which influence the photocatalytic activity.

Furthermore, the table features variations in reaction conditions, such as reaction volume and catalyst loading, suggesting efforts to optimize conditions for maximum efficiency. The impact of catalyst composition on performance is evident, with certain compositions like Bi_2WO_6/Cd and CeO_2/Cd exhibiting higher degradation efficiencies compared to others. Variations in catalyst composition, such as different molar ratios of CuO/Cd and $CuBi_2O_4$/Cd, result in differing degradation efficiencies, highlighting the importance of composition optimization. From this table suggested that the future research directions in photocatalyst development for wastewater treatment and environmental remediation, guiding efforts to explore novel compositions, optimize reaction conditions, and elucidate underlying mechanisms of photocatalytic dye degradation to enhance overall efficiency and sustainability in wastewater treatment technologies.

3.9 pH Variations

The impact of pH on the degradation rate of dyes is a critical factor in understanding the efficacy of Cd-doped V_2O_5 nanoparticles in degrading Rh-B dye. The results involved testing the degradation efficiency at different pH levels: 1, 7, and 11. The results, illustrated in Fig. 10a, revealed a gradual increase in degradation percentage with rising pH levels. This phenomenon can be attributed to the presence of active species within the nanoparticles, which exhibit enhanced degradation capabilities under acidic and alkaline conditions. In acidic environments (pH 1), the degradation rate of Rh-B reached minimum, primarily due to electrostatic interactions between the positively charged nanoparticles and the negatively charged dye molecules. This interaction, modified by the acidic medium, induces electrostatic repulsion, thereby facilitating degradation, as depicted in Fig. 10a. Additionally, the presence of low levels of Cd^{2+} ions further promotes electrostatic repulsion, augmenting the degradation process. Conversely, at neutral pH (pH 7), no significant alterations were observed in the interaction between the dye molecules and Cd-doped V_2O_5 nanoparticles, resulting in consistent degradation outcomes. However, at pH 11, a notable increase in degradation rate was observed compared to pH 2 and pH 7. The higher pH environment facilitated electrostatic attraction between the dye molecules and Cd^{2+}/V^{4+} ions, significantly enhancing catalytic activity, leading to enhanced degradation rate of Rh-B. This enhanced activity can be attributed to the increased surface area resulting from the decoration of cadmium on V_2O_5 nanoparticles, which promotes the generation of hot electrons.

Table 1 Photocatalytic comparison table of Cd-doped various metal oxide nanoparticles

Sl. No	Nanoparticles	Dye	Dye volume	Dosage	Degradation (%)	References
1	Bi_2WO_6/Cd	Rh-B	200 mL	10 mg	63%	Song et al. (2015)
2	ZnO/Cd	MB	100 mL	10 mg	80%	Zhang and Zeng (2012)
3	CeO_2/Cd	RhB	200 mL	10 mg	86.42%	Gnanam and Rajendran (2018)
4	Dimanganise/Cd	CR	50 mL	5 mg	85%	Gnanam et al. (2021)
5	Copper oxide/Cadmium sulfide	MB	100 mL	10 mg	83%	Senobari and Nezamzadeh-Ejhieh (2018)
6	ZnO/Cd	MB	50 mL	20 mg	84%%	Ghoderao et al. (2019)
7	ZnS/Cd	MO	100 mL	10 mg	78.46%	Suganya et al. (2019)
8	CuO/Cd (0.4m.mol)		100 mL	12 mg	89.50%	Wang et al. (2015)
	CuO/ Cd (1.2m.mol)				90.89%	
	CuO/ Cd (1.6m.mol)				89.22%	
	CuO/ Cd (2.0m.mol)				89.17%	
9	$CuBi_2O_4$/Cd(0.05mol)	CR	100 mL	10 mg	80%	Khan et al. (2024)
	$CuBi_2O_4$/Cd(0.15mol)	CR			86%	
10	TiO_2/Cd	CR	100 mL	30 mg	73.4%	Chandrasekar et al. (2023)
10	Cd/V_2O_5	Rh-B	100 mL	10 mg	85.91 & 94%	Present Work

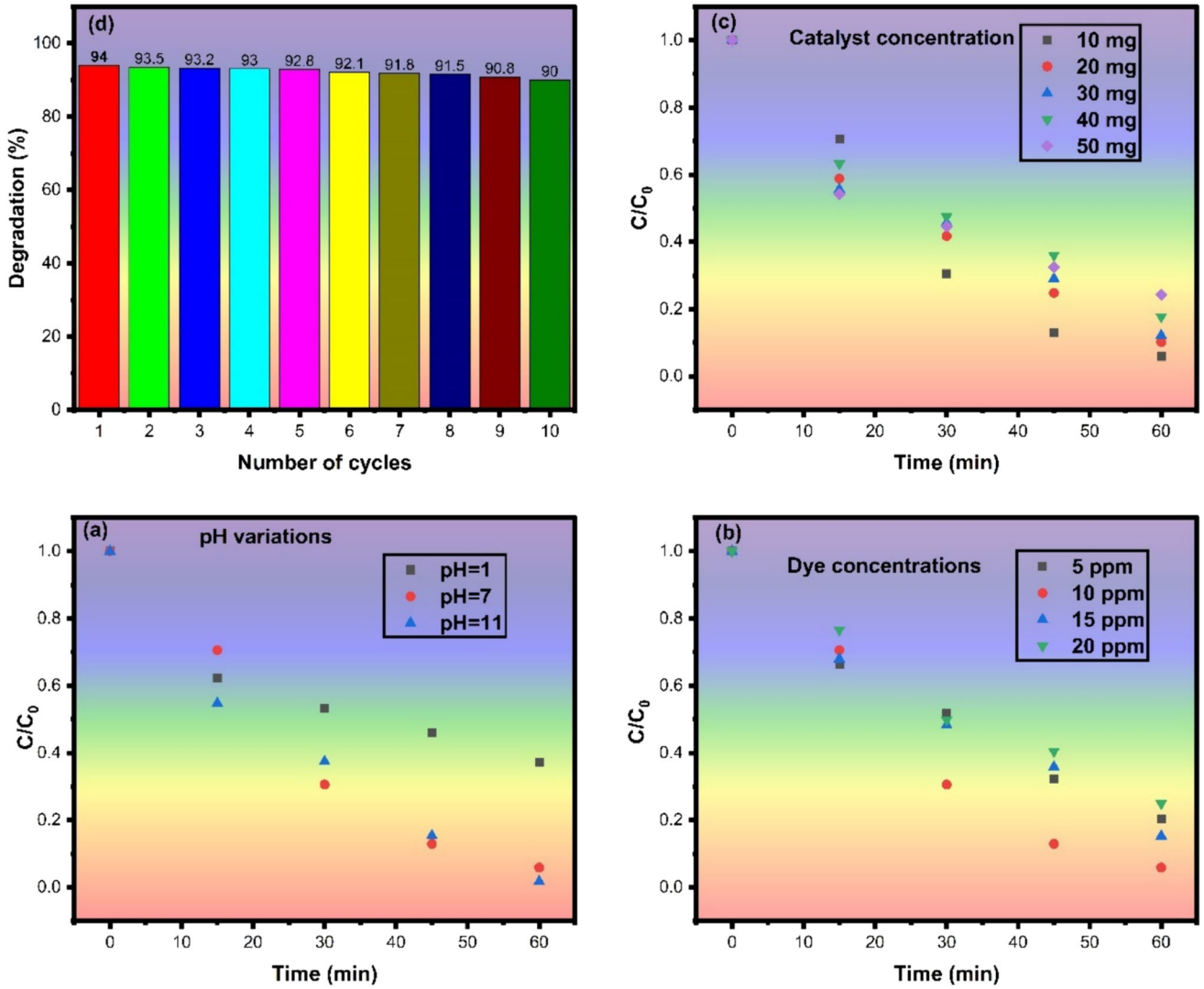

Fig. 10 Photocatalyst dye degradation of **a** different pH, Dye concentration (**b**), Catalyst concentration (**c**) and cycle study (**d**) of 10% Cd-doped V_2O_5 nanoparticles against Rh-B dye

3.10 Catalyst Variations

The influence of catalyst concentration on Rh-B dye degradation was assessed. Figure 10b depicts a gradual increase in degradation percentage with rising Cd-doped V_2O_5 concentration, peaking at 10 mg. Beyond this concentration, degradation efficiency decrease, attributed to surface area saturation. The addition of cadmium enhances surface area, with 10 mg proving optimal for catalytic activity. The obtained degradation rate was demonstrated the catalyst contributions and their surface reactions between the dye compounds.

3.11 Dye Concentrations

The effect of dye concentration, varying concentrations of Rh-B dye (ranging from 10 to 50 ppm) were examined in conjunction with Cd-doped V_2O_5 photocatalysts. Figure 10c illustrates a decrease in degradation percentage with increasing dye concentration. This degradation of dye can be attributed to the formation of hydroxyl radicals (OH·), crucial for photocatalytic degradation, which diminish as dye concentration rises. At 10 ppm, optimal conditions for OH· radical formation were observed, while higher concentrations delayed the light penetration and occupied active sites, limiting radical generation and thereby decreasing degradation efficiency.

3.12 Cycle Study

The reusability of Cd-doped V_2O_5 nanoparticles in Rh-B dye degradation was evaluated over ten cycles (Fig. 10d). Results demonstrated consistent degradation, with a slight decrease from 94 to 90% after ten cycles. The stability of

Cd-doped V_2O_5 nanoparticles suggests their viability for extended use in wastewater treatment, with minimal degradation observed due to factors such as surface washing, pore obstruction, and dye molecule occupation. These results emphasize the potential of synthesized Cd-doped V_2O_5 nanoparticles as efficient catalysts for wastewater remediation.

4 Conclusion

The facile co-precipitation method successfully synthesized Cd-doped V_2O_5 nanoparticles, as confirmed by FE-SEM with EDX and TEM analyses, revealing the effective incorporation of Cd^{2+} into the V_2O_5 atomic lattice. At 10 M% Cd^{2+}, significant enhancements in optical properties were observed, characterized by optical absorption at 650 nm and a bandgap value of 1.88 eV, demonstrating promising catalytic applicability across UV and visible spectra. FTIR and photoluminescence analyses provided further insights into functional groups, charge dynamics, and cationic transitions, while XPS analyses validated the presence of Cd, V, and O compounds, affirming their multivalency and stabilized particle characteristics. The catalytic activity of 10 M% Cd-doped V_2O_5 nanoparticles in Rhodamine B dye degradation showed a remarkable 94% degradation rate within 60 min. This efficiency was attributed to the Cd dopant's role in increasing surface area, inducing photoexcitation, preventing atomic agglomeration, and promoting electron donation-mediated radical formation, thereby enhancing photocatalytic performance. The study highlights the critical influence of pH, catalyst concentration, and dye concentration on Rh-B dye degradation efficiency using Cd-doped V_2O_5 nanoparticles as catalysts. Optimal performance necessitates balancing pH-dependent electrostatic interactions and avoiding surface area saturation. These findings underscore the potential of Cd-doped V_2O_5 nanoparticles as highly effective catalysts, supporting their application in diverse catalytic processes. The scientific significance lies in their tailored optical and electronic properties, which enable efficient utilization in environmental and industrial applications requiring advanced catalytic materials.

Acknowledgements A. Remila Research Scholar (Reg. No: 20113042132010) drew the thanks to Department of Physics, Holy Cross College (Autonomous), Nagercoil-629004 and Manonmaniam Sundaranar University, Abishekapatti, Tirunelveli-627012, Tamil Nadu, INDIA

Funding No funding was received to assist with the preparation of this manuscript.

Data Availability All research data associated with the manuscript.

Declarations

Conflict of interest The author has no conflict of interest.

References

Abd El-Ghany WA, Ismail AM, Khattari ZY, Teleb NH (2024) Optimization of the structural, optical and electrical properties of PVA/V_2O_5 for shielding applications. Radiat Phys Chem 219:111656. https://doi.org/10.1016/j.radphyschem.2024.111656

Alqahtani A, Shkir M, Khan A, Alkallas FH, Gouider Trabelsi AB, AlFaify S, Khan FS, Kapoor M (2024) V2O5: Cu thin films-based device fabrication for high-performance photosensing application. Opt Mater 150:115283. https://doi.org/10.1016/j.optmat.2024.115283

Alsharyani AK, Muruganandam L (2024) Fabrication of zinc oxide nanorods for photocatalytic degradation of docosane, a petroleum pollutant, under solar light simulator. RSC Adv 14:9038–9049. https://doi.org/10.1039/D4RA00672K

Anandan K, Rajendran V (2011) Morphological and size effects of NiO nanoparticles via solvothermal process and their optical properties. Mater Sci Semicond Process 14(1):43–47. https://doi.org/10.1016/j.mssp.2011.01.001

Bansal S, Purnima J (2024) Photocatalytic evaluation of chitosan and its derivative coated vanadium pentoxide nanoparticles for photodegradation of methylene blue. In: E3S Web of Conferences, vol 488, p 02010 https://doi.org/10.1051/e3sconf/202448802010

Bhakare MA, Dhumal PS, Bondarde MP, Lokhande KD, Some S (2024) Transformation of waste into valuable materials: utilizing waste printer powder to remove hazardous organic dye and pharmaceutical pollutants from wastewater. Colloids Surf A Physicochem Eng Aspects 685:133196. https://doi.org/10.1016/j.colsurfa.2024.133196

Bhuvaneswari K, Jintae Lee A, Viji MS (2024) Strategic rationalization for improved photocatalytic decomposition of toxic pollutants: Immobilizing Bi_2Te_3 nanorods and V_2O_5 nanoparticles over MoS_2 nanosheets. Spectrochim Acta A Mol Biomol Spectrosc 304:123400. https://doi.org/10.1016/j.saa.2023.123400

Boukoussa B, Cherdouane KR, Zegai R, Mokhtar A, Hachemaoui M, Issam I, Iqbal J, Patole SP, Zeggai FatimaZohra, Hamacha R, Abboud M (2024) Preparation of activated carbon-metal nanoparticle composite materials for the catalytic reduction of organic pollutants. Surf Interfaces 44:103622. https://doi.org/10.1016/j.surfin.2023.103622

Chamarro MA, Voliotis V, Grousson R, Lavallard P, Gacoin T, Counio G, Boilot P, Cases R (1996) Optical properties of Mn-doped CdS nanocrystals. J Cryst Growth 159(1–4):853–856. https://doi.org/10.1016/0022-0248(95)00863-2

Chandrasekar M, Subash M, Perumal V, Aravindan S, Uthrakumar R, Inmozhi C, Babujanarthanam R, Kaviyarasu K (2023) Specific charge separation of Cd doped TiO_2 photocatalysts for energy applications. Mater Sci Energy Technol 6:472–483. https://doi.org/10.1016/j.mset.2023.04.010

Cleret de Langavant C, Oh J, Lochon F, Tusseau-Nenez S, Ponsinet V, Baron A, Gacoin T, Kim J (2024) Near-infrared dual-band lspr coupling in oriented assembly of doped metal oxide nanocrystal platelets. Nano Lett 24(10):3074–3081. https://doi.org/10.1021/acs.nanolett.3c04849

Dawi EA, Mustafa E, Padervand M, Ashames A, Hajiahmadi S, Saleem L, Baghernejad M, Nur O, Willander M (2023) Ag/AgCl decorated ionic liquid@ tantalum pentoxide nanostructures:

fabrication, photocatalytic activity and cytotoxicity effects against human brain tumor cells. J Inorg Organomet Polym Mater 33:2647–2660. https://doi.org/10.1007/s10904-023-02693-x

Farooque Lanjwani M, Tuzen M, Yar Khuhawar M, Saleh TA (2024) Trends in photocatalytic degradation of organic dye pollutants using nanoparticles: a review. Inorg Chem Commun 159:111613. https://doi.org/10.1016/j.inoche.2023.111613

Ghannam H, Rossi Z, Haloui S, Elmouwahidi A, Abdesamad A, Teddy T, Diani M, Chahboun A (2024) Effect of manganese and Zinc co-dopants on electrochemical properties of vanadium oxide (V_2O_5) based electrode: application for supercapacitor. Res Sq. https://doi.org/10.21203/rs.3.rs-3856870/v1

Ghoderao KP, Jamble SN, Kale RB (2019) Hydrothermally synthesized Cd-doped ZnO nanostructures with efficient sunlight-driven photocatalytic and antibacterial activity. J Mater Sci Mater Electron 30:11208–11219. https://doi.org/10.1007/s10854-019-01466-y

Gnanam S, Rajendran V (2018) Facile sol-gel preparation of Cd-doped cerium oxide (CeO_2) nanoparticles and their photocatalytic activities. J Alloy Compd 735:1854–1862. https://doi.org/10.1016/j.jallcom.2017.11.330

Gnanam S, Gajendiran J, Ashokkumar R, Ramachandran K, Ramya JR (2021) Cd doped-alpha-dimanganese trioxide nanoparticles: synthesis, structural, morphological, optical, luminescent, magnetic, photocatalytic and antibacterial characterization. J Mol Struct. https://doi.org/10.1016/j.molstruc.2020.129846

Gorsi AT, Mansoor S, Javed M, Sohail MT, Bahadur A, Iqbal S, Mahmood S, Alshalwi M, Qamar MA, Qayyum MA (2024) Sunlight-active, S-g-C_3N_4 boosts Ni-doped $ZnFe_2O_4$ photocatalysts for efficient organic pollutants degradation. Opt Mater 150:115181. https://doi.org/10.1016/j.optmat.2024.115181

Goudarzi F, Soleymani M (2019) Synthesis, characterization and application of V_2O_5/S-doped graphitic carbon nitride nanocomposite for removing of organic pollutants. Chem Select 4(46):13420–13753. https://doi.org/10.1002/slct.201903885

Habibi MH, Rahmati MH (2014) Fabrication and characterization of ZnO@CdS core–shell nanostructure using acetate precursors: XRD, FESEM, DRS, FTIR studies and effects of cadmium ion concentration on band gap. Spectrochim Acta Part A Mol Biomol Spectrosc 133:13–18. https://doi.org/10.1016/j.saa.2014.04.110

Hota G, Idage SB, Khilar KC (2007) Characterization of nano-sized CdS–Ag_2S core-shell nanoparticles using XPS technique. Colloids Surf A 293(1–3):5–12. https://doi.org/10.1016/j.colsurfa.2006.06.036

Hussain E, Ishaq A, Abid MZ, Zaryab Waleed M, Rauf A, Jin R, Rafiq K (2024) Sunlight-driven hydrogen generation: acceleration of synergism between Cu–Ag cocatalysts on a CdS system. ACS Appl Energy Mater 7(5):1914–1926. https://doi.org/10.1021/acsaem.3c03010

Jana NR, Gearheart L, Murphy CJ (2001) Seed-mediated growth approach for shape-controlled synthesis of spheroidal and rod-like gold nanoparticles using a surfactant template. Adv Mater 13(18):1389–1393. https://doi.org/10.1002/1521-4095(200109)13:18%3c1389::AID-ADMA1389%3e3.0.CO;2-F

Javdani-Mallak A, Iman Salahshoori I (2024) Environmental pollutants and exosomes: a new paradigm in environmental health and disease. Sci Total Environ 925:171774. https://doi.org/10.1016/j.scitotenv.2024.171774

Jenifer A, Sriram S (2023) Enhanced photocatalytic organic dye degradation activities of pristine and Zn-doped V_2O_5 nanoparticles. Appl Surf Sci 611:155629. https://doi.org/10.1016/j.apsusc.2022.155629

Jia Z, Yue L, Zheng Y, Zhude Xu (2008) Rod-like zinc oxide constructed by nanoparticles: synthesis, characterization and optical properties. Mater Chem Phys 107(1):137–141. https://doi.org/10.1016/j.matchemphys.2007.06.061

Jia X, Yan K, Sun Y, Chen Y, Tang Y, Pan J, Wan P (2024) Solvothermal guided V_2O_5 microspherical nanoparticles constructing high-performance aqueous zinc-ion batteries. Materials 17(7):1660. https://doi.org/10.3390/ma17071660

Khan J, Khan AU, Khan Y, Wei Y, Khan QU, Al-Saeedi SI (2024) Controlled synthesis of Cadmium doped $CuBi_2O_4$ nanorods with rapid and synergistic visible light photocatalytic performance. Chem Eng Sci 293:120025. https://doi.org/10.1016/j.ces.2024.120025

Kishan Chand TR, Kalpana HM, Satish TN (2024) Effect of thickness and annealing on electrical characteristics of cerium oxide-doped vanadium oxide (CeO_2:V_2O_5) thin film for sensor application. J Mater Sci Mater Electron 35:616. https://doi.org/10.1007/s10854-024-12388

Kočišová E, Kuzminova A, Kuižová A, Adéla Hanková T, Košutová MP, Kylián O (2024) V_2O_5 nanoparticle films as a platform for plasmon-free surface-enhanced Raman spectroscopy. Ceram Int 50(7):10026–10033. https://doi.org/10.1016/j.ceramint.2023.12.314

Kumar SRA, Mary DV, Josephine GSA, Sivasamy A (2024) Hydrothermally synthesized WO3:CeO2 supported gC3N4 nanolayers for rapid photocatalytic degradation of azo dye under natural sunlight. Inorg Chem Commun 164:112366. https://doi.org/10.1016/j.inoche.2024.112366

Le HA, Chin S, Park E, Bae G, Jurng J (2012) Chemical vapor synthesis and physico-chemical properties of V_2O_5 nanoparticles. Chem Vap Depos 18(1–3):6–9. https://doi.org/10.1002/cvde.201104307

Le TK, Kang M, Kim SW (2019) Morphology engineering, room-temperature photoluminescence behavior, and sunlight photocatalytic activity of V_2O_5 nanostructures. Mater Charact 153:52–59. https://doi.org/10.1016/j.matchar.2019.04.046

Luo Z, Zhiming Wu, Xiangdong Xu, Mingjun Du, Wang T, Jiang Y (2010) Impact of substrate temperature on the microstructure, electrical and optical properties of sputtered nanoparticle V_2O_5 thin films. Vacuum 85(2):145–150. https://doi.org/10.1016/j.vacuum.2010.05.001

Minisha S, Johnson J, Mohammad S, Gupta JK, Aftab S, Alothman AA, Lai W-C (2024) Visible light photocatalytic degradation of environmental pollutants using Zn-doped NiO nanoparticles. Water 16(2):340. https://doi.org/10.3390/w16020340

Mishra A (2024) Structural characterization of CdS-PVA nanocomposites in view of their applications in solar cells. Vidhyayana Int Multidiscip Peer-Rev E-J 9(2):36. https://doi.org/10.58213/vidhyayana.v9isi2

Morsy M, Samir M, Al-Qahtani A, Aslsaiari R, Alsaiari A, Kamoun E, Ali AI, Ramzy G (2024) Advantages incorporating V_2O_5 nanoparticles into PMMA composite membranes for the structural, optical, electrical, and mechanical properties for conductive polymeric membrane applications. Mater Adv 5(8):3297. https://doi.org/10.1039/D3MA01108A

Naderahmadian A, Eftekhari-Sis B, Jafari H, Zirak M, Padervand M, Mahmoudi G, Samadi M (2023) Cellulose nanofibers decorated with SiO_2 nanoparticles: green adsorbents for removal of cationic and anionic dyes; kinetics, isotherms, and thermodynamic studies. Int J Biol Macromol 247:125753. https://doi.org/10.1016/j.ijbiomac.2023.125753

Naeema N, Kadhim OJ, Abdullah NJ, Aldhuhaibat MJR, Bakhtiar H, Salim AA (2023) Shielding performance of metal oxide nanoparticles-doped polypropylene composites against gamma

rays and neutrons exposure. Radiat Phys Chem 216:111461. https://doi.org/10.1016/j.radphyschem.2023.111461

Nivetha S, Srivalli T, Sathya PM, Mohan H, Karthi N, Muralidharan K, Ramalingam V (2024) Nickel-doped vanadium pentoxide (Ni@V_2O_5) nanocomposite induces apoptosis targeting PI3K/AKT/mTOR signaling pathway in skin cancer: an in vitro and in vivo study. Colloids Surf B 234:113763. https://doi.org/10.1016/j.colsurfb.2024.113763

Odhaib AJ, Pirsa S, Mohtarami F (2024) Biodegradable film based on barley sprout powder/pectin modified with quercetin and V_2O_5 nanoparticles: investigation of physicochemical and structural properties. J Heliyon 10(3):e25448. https://doi.org/10.1016/j.heliyon.2024.e25448

Padervand M, Rhimi B, Wang C (2020) One-pot synthesis of novel temary Fe3N/Fe2O3/C3N4 photocatalyst for efficient removal of rhodamine B and CO2 reduction. J Alloy Compd 852:156955. https://doi.org/10.1016/j.jallcom.2020.156955

Pandarinath MA, Madhuri JH, Chanakya N, Devi CS, Upender G (2024) Spectroscopic and thermal investigations on Zn^{2+} and Ba^{2+} ions modified $30TeO_2$-$39.5B_2O_3$-(30-x)ZnO-xBaO-$0.5V_2O_5$ ($0 \leq x \leq 30$ mol %) glass system. Spectrochim Acta Part A Mol Biomol Spectrosc 313:124088. https://doi.org/10.1016/j.saa.2024.124088

Parvathiraja C, Shailajha S (2023) High- performance visible light photocatalyst antibacterial applications of ZnO and plasmonic-decorated ZnO nanoparticles. Appl Nanosci 13(6):3659–3675. https://doi.org/10.1007/s13204-022-02488-5

Qu C, Chen J, Mortimer M, Wu Y, Cai P, Huang Q (2022) Humic acids restrict the transformation and the stabilization of Cd by iron (hydr)oxides. J Hazard Mater 430:128365. https://doi.org/10.1016/j.jhazmat.2022.128365

Raja VR, Rosaline DR, Suganthi A, Rajarajan M (2018) Facile sonochemical synthesis of Zn_2SnO_4-V_2O_5 nanocomposite as an effective photocatalyst for degradation of Eosin Yellow. Ultrasonics Sonochem 44:310–318. https://doi.org/10.1016/j.ultsonch.2018.02.043

Rajalakshmi S, Pitchaimuthu S, Kannan N, Velusamy P (2014) Photocatalytic effect of β-cyclodextrin on semiconductors for the removal of acid violet dye under UV light irradiation. Desalin Water Treat 52(16–18):3432–3444. https://doi.org/10.1080/19443994.2013.809024

Remila A, Shally V, Parvathiraja C, Darwin T, Dharshini MP, Jayam TG, Siddiqui MR (2024) Superior performance of nickel doped vanadium pentoxide nanoparticles and their photocatalytic, antibacterial and antioxidant activities. Res Chem Intermed 50:3009–3031. https://doi.org/10.1007/s11164-024-05316-3

Ren H, Labidi A, Sial A, Gao T, Xu X, Liang J, Wang C (2024) Carbon quantum dots modified Z and S-Scheme heterojunctions for pharma ceutical contaminants photodegradation: State- of-the-art, benefits, and limitations. Sep Purif Technol 346:127508. https://doi.org/10.1016/j.seppur.2024.127508

Sahoo S, Vishva Jain DV, Shah RD, Pathak A (2024) Effect of Mo doping in vanadium pentoxide (V_2O_5) for dye degradation. J Cryst Growth 627:127491. https://doi.org/10.1016/j.jcrysgro.2023.127491

Salleh NKM, Aziz F, Mohtar SS, Mohammad AM, Mhamad SA, Yusof N, Jaafar J, Salleh WNW (2024) Strategies to improve the antimicrobial properties of metal-oxide based photocatalytic coating: a review. Progr Org Coat 187:108183. https://doi.org/10.1016/j.porgcoat.2023.108183

Sammed KA, Kumar A, Farid A, Zhang W, Akbar AR, Ali M, Ajmal S, Yasin G, Ullah N, Pan L, Zhao W (2024) Exploration of the role of oxygen-deficiencies coupled with Ni-doped V_2O_5 nanosheets anchored on carbon nanocoils for high-performance supercapacitor device. Chem Eng J 486:150388. https://doi.org/10.1016/j.cej.2024.150388

Senobari S, Nezamzadeh-Ejhieh A (2018) A comprehensive study on the photocatalytic activity of coupled copper oxide-cadmium sulfide nanoparticles. Spectrochim Acta Part A Mol Biomol Spectrosc 196:334–343. https://doi.org/10.1016/j.saa.2018.02.043

Shang L, Tong B, Yu H, Waterhouse GIN, Zhou C, Zhao Y, Tahir M, Wu L-Z, Tung C-H, Zhang T (2016) CdS nanoparticle-decorated Cd nanosheets for efficient visible light-driven photocatalytic hydrogen evolution. Adv Energy Mater. https://doi.org/10.1002/aenm.201501241

Singh A, Goswami P, Koch B et al (2024) Study of human osteosarcoma cell line growth, hemocompatibility, in-vitro analysis and physical properties of V_2O_5 substituted borosilicate glass. SILICON. https://doi.org/10.1007/s12633-024-02849-5

Song XC, Li WT, Huang WZ et al (2015) Enhanced photocatalytic activity of cadmium-doped Bi_2WO_6 nanoparticles under simulated solar light. J Nanopart Res 17:134. https://doi.org/10.1007/s11051-015-2945-1

Suganya S, Jothibas M, Jeyakumar SJ (2019) Solid state synthesis of cadmium doped ZnS with excellent photocatalytic activity and enhanced visible light emission. J Mater Sci Mater Electron 30:7916–7927. https://doi.org/10.1007/s10854-019-01113-6

Venkatesan A, Krishna Chandar N, Arjunan S, Marimuthu KN, Mohan Kumar R, Jayavel R (2013) Structural, morphological and optical properties of highly monodispersed PEG capped V_2O_5 nanoparticles synthesized through a non-aqueous route. Mater Lett 91:228–231. https://doi.org/10.1016/j.matlet.2012.09.117

Venu Gopal VR, Kamila S (2017) Effect of temperature on the morphology of ZnO nanoparticles: a comparative study. Appl Nanosci 7:75–82. https://doi.org/10.1007/s13204-017-0553-3

Vijayalakshmi S, Venkataraj S, Jayavel R (2008) Characterization of cadmium doped zinc oxide (Cd: ZnO) thin films prepared by spray pyrolysis method. J Phys D Appl Phys 41(24):245403. https://doi.org/10.1088/0022-3727/41/24/245403

Vinothini A, Conceptulaization AM, Arulkumar E, Vedhi C, Thanikaikarasan S (2024a) Green route synthesis of transition metal doped V_2O_5 nanoparticles, with emerging biomedical applications. Results Chem 7:101373. https://doi.org/10.1016/j.rechem.2024.101373

Vinothini A, Conceptulaization AM, Arulkumar E, Vedhi C, Thanikaikarasan S (2024b) Green route synthesis of transition metal doped V_2O_5 nanoparticles with emerging biomedical applications. Results Chem 7:101373. https://doi.org/10.1016/j.rechem.2024.101373

Wang Y, Jiang T, Meng D, Wang D, Meihua Yu (2015) Synthesis and enhanced photocatalytic property of feather-like Cd-doped CuO nanostructures by hydrothermal method. Appl Surf Sci 355:191–196. https://doi.org/10.1016/j.apsusc.2015.07.122

Wang C-C, Chia-Lun Lu, Shieu F-S, Shih HC (2021) Structure and photoluminescence properties of thermally synthesized V_2O_5 and Al-doped V_2O_5 nanostructures. Materials 14(2):359. https://doi.org/10.3390/ma14020359

Wang J, Zheng F, Jia D, Li Y, Niu Y, Mao X, Zhen Q, Yi Yu (2024) Hydrothermal preparation of porous NiO nanoflake arrays@V_2O_5 nanoparticles composite for high performance supercapacitive electrode material. J Alloy Compd 976:172955. https://doi.org/10.1016/j.jallcom.2023.172955

Xu X, Lu Y, Liu D et al (2024) Highly efficient photoelectrochemical aptasensor based on CdS/CdTe QDs co-sensitized TiO_2 nanoparticles designed for thrombin detection. Microchim Acta 191:216. https://doi.org/10.1007/s00604-024-06279-3

Zhang D, Zeng F (2012) Visible light-activated cadmium-doped ZnO nanostructured photocatalyst for the treatment of methylene blue dye. J Mater Sci 47:2155–2161. https://doi.org/10.1007/s10853-011-6016-4

Zolfagharpour HR, Sharafati A, Hosseinzadeh M (2024) Catalytic pyrolysis of sugarcane bagasse using V_2O_5 nanoparticles in an auger reactor. J Anal Appl Pyrolysis 177:106357. https://doi.org/10.1016/j.jaap.2024.106357